Volume 13
Number 3
21 January 2022
Pages 583–850

Chemical Science

rsc.li/chemical-science

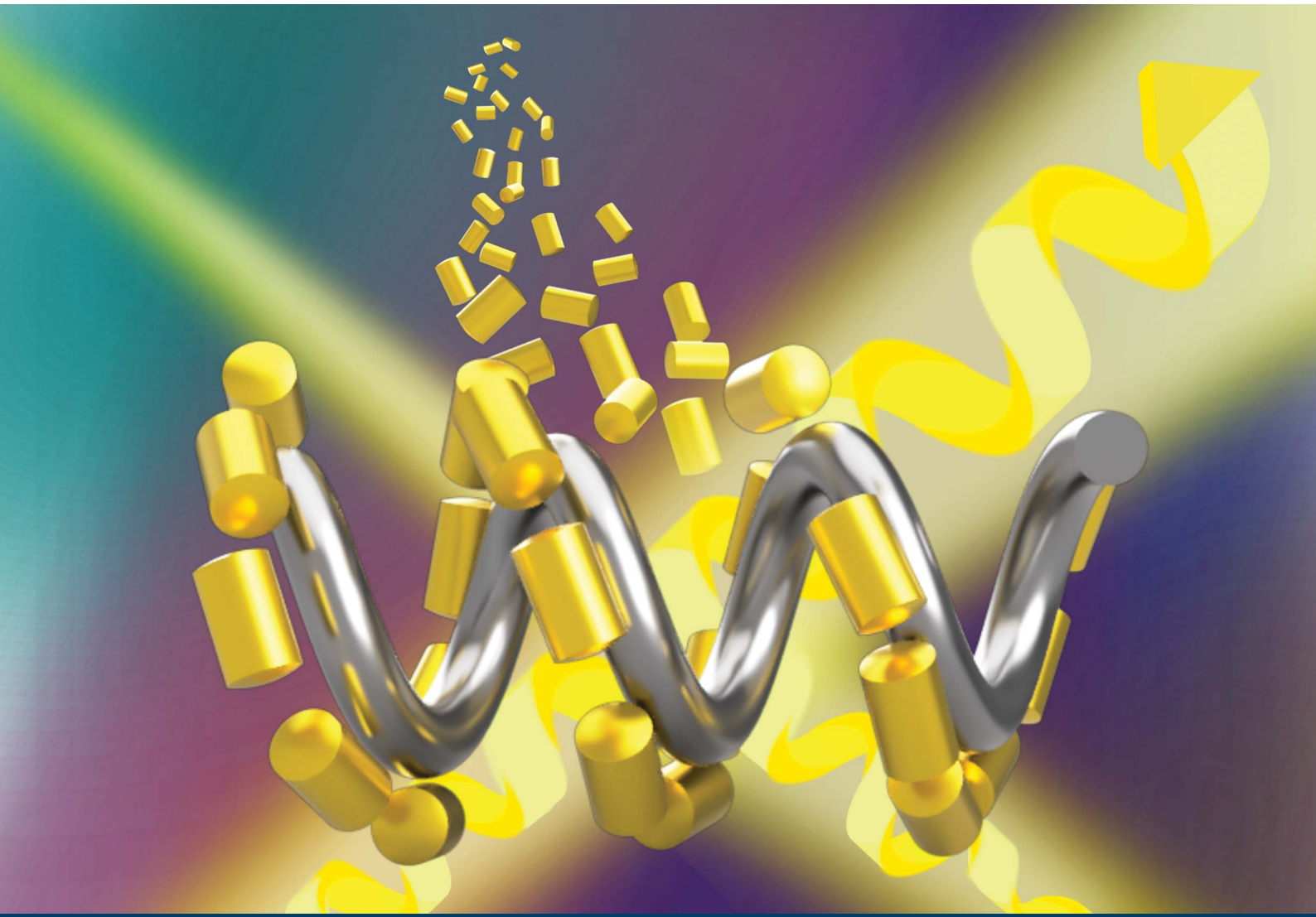

Themed issue: Chiral Nanomaterials

ISSN 2041-6539

ROYAL SOCIETY OF CHEMISTRY

REVIEW ARTICLE
Luis M. Liz-Marzán *et al.*
Template-assisted self-assembly of achiral plasmonic nanoparticles into chiral structures

Chemical Science

ROYAL SOCIETY OF CHEMISTRY

REVIEW

View Article Online
View Journal | View Issue

Cite this: *Chem. Sci.*, 2022, **13**, 595

Template-assisted self-assembly of achiral plasmonic nanoparticles into chiral structures

David Vila-Liarte,[ab] Nicholas A. Kotov[cd] and Luis M. Liz-Marzán *[abe]

The acquisition of strong chiroptical activity has revolutionized the field of plasmonics, granting access to novel light–matter interactions and revitalizing research on both the synthesis and application of nanostructures. Among the different mechanisms for the origin of chiroptical properties in colloidal plasmonic systems, the self-assembly of achiral nanoparticles into optically active materials offers a versatile route to control the structure–optical activity relationships of nanostructures, while simplifying the engineering of their chiral geometries. Such unconventional materials include helical structures with a precisely defined morphology, as well as large scale, deformable substrates that can leverage the potential of periodic patterns. Some promising templates with helical structural motifs like liquid crystal phases or confined block co-polymers still need efficient strategies to direct preferential handedness, whereas other templates such as silica nanohelices can be grown in an enantiomeric form. Both types of chiral structures are reviewed herein as platforms for chiral sensing: patterned substrates can readily incorporate analytes, while helical assemblies can form around structures of interest, like amyloid protein aggregates. Looking ahead, current knowledge and precedents point toward the incorporation of semiconductor emitters into plasmonic systems with chiral effects, which can lead to plasmonic–excitonic effects and the generation of circularly polarized photoluminescence.

Received 21st June 2021
Accepted 2nd September 2021

DOI: 10.1039/d1sc03327a

rsc.li/chemical-science

[a]*CIC biomaGUNE, Basque Research and Technology Alliance (BRTA), Paseo de Miramon 194, 20014, Donostia San Sebastián, Spain. E-mail: llizmarzan@cicbiomagune.es*

[b]*Centro de Investigación Biomédica en Red, Biomateriales, Bioingeniería y Nanomedicina (CIBER-BBN), Spain*

[c]*Department of Chemical Engineering, Materials Science, Department of Biomedical Engineering, University of Michigan, Ann Arbor, USA. E-mail: kotov@umich.edu*

[d]*Biointerfaces Institute, University of Michigan, Ann Arbor, USA*

[e]*Ikerbasque, Basque Foundation for Science, 48013 Bilbao, Spain*

David Vila-Liarte received his B.S. and Master's degrees in nanoscience and nanotechnology from the Autonomous University of Barcelona (2019). During this time, he helped to develop the templated self-assembly of gold nanorods and later implemented it on perovskite nanocrystals, as his Master's thesis at the Institute of Materials Science of Barcelona (ICMAB-CSIC). In 2019, he joined the Bionanoplasmonic's group, led by Prof. Liz-Marzán at CIC biomaGUNE (San Sebastián, Spain) as a PhD student. His research interests are focused on plasmonic systems with optical activity.

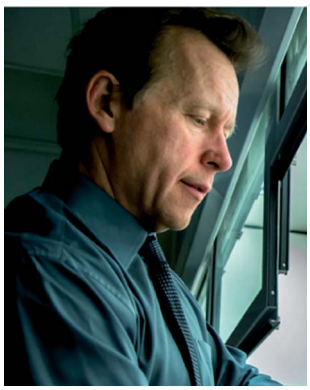

Nicholas Kotov graduated from Moscow State University with a PhD focused on bioinspired harvesting of solar energy. His postdoctoral studies at Syracuse University encompassed the synthesis of biomimetic nanocomposites. Transitioning to Oklahoma State University, he established a research program on the self-assembly of nanostructures. Nicholas is currently the Irving Langmuir Professor of Chemical Sciences and Engineering at the University of Michigan, heading a laboratory and an international team of scientists working on biomimetic nanostructures. Chiral nanoparticles are central to biomimetic nanomaterials with high significance to physics, chemistry, and biology. Nicholas is a founder of five startups and a passionate advocate for scientists with disabilities.

Introduction

An object is called chiral if it cannot be superimposed with its mirror image by means of rotational or translational operations. This foundational geometrical property gives rise to optical activity, *i.e.* the rotation of the plane of polarization of incident light. Accordingly, chiral materials interact differently with light that is right- or left-circularly polarized, having distinct extinction cross sections for each polarization. The most common choice for the characterization of such differences in absorbance is circular dichroism (CD) spectroscopy, even though optical activity can also be detected by other methods like optical rotatory dispersion or Raman optical activity.[1] Not only biomolecules like hydrocarbons or amino acids, but also noble metal nanomaterials, which owe their outstanding optical properties to coherent oscillations of conduction electrons in plasmon resonance modes, can display optical activity.[2,3] The fabrication of a wide variety of chiral plasmonic nanostructures and meta-surfaces has been demonstrated by both top-down[4] and bottom-up[5] fabrication techniques,[6] finding novel applications[7,8] in photonics,[9,10] bioimaging[11] or biosensing.[12,13]

When it comes to colloidal plasmonic nanoparticles (NPs) synthesized by wet chemistry methods, optical properties can be tuned at the synthesis stage – through their composition, size and shape – or by their subsequent self-assembly, either in solution[5,14] or on templates.[15] These parameters influence the wavelength at which the plasmonic excitation is in resonance with incident electromagnetic radiation. Such a dependency can be seen in terms of (i) the nanoscale spatial confinement of the electron cloud, plasmonic modes supported by the specific NP geometry; (ii) a strong electromagnetic field enhancement at the vicinity of the NPs; (iii) sensitivity to the environment, allowing dipole–dipole interactions and hybridization of plasmon resonance modes through coupling with other plasmonic entities. In this context, three different mechanisms may enable a plasmonic system to acquire chiroptical properties, which has become a breakthrough in the toolbox of plasmonic NPs. Perhaps the most intuitive mechanism is related to optical activity being induced by an asymmetric NP shape of molecular segments on their surface.[16,17] The seeded-growth concept has demonstrated the preparation of gold NPs with mirror-asymmetric geometry,[18] using either chiral amino acids,[19] chiral co-surfactant micelles,[20] or photon-to-particle chirality transfer[21,22] to direct the seeded-growth on initial cube-, rod-, or sphere-shaped seeds, respectively. Besides the chiral shapes of the NP cores as the source of intrinsic optical activity in plasmonic systems, other mechanisms have been widely exploited during the past two decades.[7,23] On one hand, plasmonic chirality can be induced through photonically driven dipole–dipole interactions between plasmonic NPs and chiral molecules adsorbed on their surface,[24] while weak molecular CD can also be enhanced by strong chiral electromagnetic fields in the vicinity of NPs.[25,26] On the other hand, plasmonic systems can acquire chirality – even in the absence of chiral adsorbates – from the mutual interaction in chiral assemblies (superstructures) produced by plasmonic units positioned in 3D space following a chiral pattern.[5] Indeed, chirality can be induced in symmetric arrangements of isotropic NPs if their constituents feature differences in size[27] or composition,[28] whereas a small dihedral angle is also sufficient to break the symmetry in the assemblies of anisotropic NPs, as has been shown for dimers[29,30] and tetramers[31] of gold nanorods. In both cases circular dichroism can be measured and a sensitive geometry–chiroptical activity relationship can be maintained. Therefore, plasmonic NPs organized into chiral assemblies display collective optical activity as a consequence of collective plasmon coupling among their building units. Since the use of chiral building blocks to create chiral superstructures has only been reported for a limited number of inorganic NPs, like truncated tetrahedral quantum dots[32] or CdTe NPs functionalized with chiral surface ligands,[33] this review will focus on the chiroptical activity originating from the assemblies of achiral plasmonic NPs, discussing recent progress in the development of unconventional templates.

At the forefront of chiral geometries, helicoids are the most visually appealing and easily recognized chiral shapes, with high anisotropy and the potential advantage of including periodicity.[34] Helicoidal motifs spontaneously emerge in a wide variety of systems,[35] some of them being potential templates to induce the self-assembly of plasmonic NPs.[36,37] As dictated by the sought interactions with the template of choice, helices, spirals, twisted ribbons and other helicoids might incorporate a large number of NPs. Plasmon coupling between NPs excited by incident photons would generate collective optical activity[38] with a specific CD sign, spectral position and intensity, depending on geometrical parameters[39,40] like the pitch, NP dimensions and interparticle distances, among others. While few-NP chiral systems were first demonstrated with PCR-based assembly protocols,[5] and great precision can be achieved by using DNA origami templates,[41,42] larger-scale ensembles have also been achieved using other materials for templating chiral self-assembly. Established examples include the use of peptides,[43,44] chiral fibers,[45] or even bacteria,[46] while new

Luis Liz-Marzán has been an Ikerbasque Professor and Scientific Director of CIC biomaGUNE, in San Sebastián (Spain), since 2012. He graduated in chemistry from the University of Santiago de Compostela, was a postdoctoral researcher at Utrecht University and a Professor at the University of Vigo (1995–2012), as well as a visiting professor at various research institutions worldwide. Liz-Marzán is considered a pioneer in the colloidal synthesis and self-assembly of metal nanocrystals, as well as the characterization and application of their plasmonic properties. His recent research focuses on the biomedical applications of plasmonic nanostructures.

potential candidates like semiconductor helices are being introduced.[47] In such drastically different materials, slightly twisted orientations of assembled NPs – even at single degree angles – are a sufficient source of asymmetry to induce a collective chiroptical response toward impinging circularly polarized light. While discussion about the fabrication of chiral assemblies cannot ignore the significant differences that arise between diverse state-of-the-art systems, the actual chiroptical performance relies on a property that is not affected by concentration, to establish a ground for comparison. The optical anisotropy factor for polarization rotation (also referred to as the *g*-factor) accounts for the optical activity normalized by absorbance.[48]

All of these thoughts will be at the center of our discussion below. Different materials that can be implemented as templates for the self-assembly of plasmonic NPs into CD-active systems will be reviewed as included in two main groups: (i) patterned templates and (ii) helical templates. Within each category, the generation of chiroptical activity through innovative procedures and unconventional templates will be evaluated. Recent contributions will be reviewed, paying attention to practical aspects and remaining challenges to be addressed, including the reversibility or the transfer of chiral materials into working devices. Next, the relationship between the nanostructure and the resulting optical activity will be addressed. Future directions will be presented in the context of hybrid plasmonic–excitonic systems.[49,50] These chiral materials can reveal unique topological effects for energy flows,[51] circularly polarized luminescence (CPL), the Bychkov–Rashba effect, and circularly polarized light scattering also known as differential scattering.[52]

Templated self-assembly of plasmonic NPs into chiral morphologies

Asymmetry through confinement

When it comes to the use of templates, 1D confinement imposed by cylindrical features can give access to different symmetry breaking scenarios. One example is the tilted deposition of Au onto rod-like nanoposts.[53] In the case of colloids, the self-assembly of achiral NPs can benefit from the steric constraints imposed by a cylindrical cavity to achieve long-range, helical arrangements. In fact, the exact configuration of densely packed spheres under cylindrical confinement depends strongly on the ratio between the diameters of the channel and the spheres.[54] According to such a geometrical restriction, confined spheres can spontaneously adopt helical structures as the most efficient packing, which is driven by excluded volume interactions.[54,55]

This principle is exemplified by soft materials like microtubes formed by the assembly of sodium dodecylsulfate and beta-cyclodextrin complexes,[56] which allow the formation of micron-sized helical assemblies of silica or polystyrene (PS) particles.[57] Although such a system can display dynamic responses like temperature sensitivity, pointing toward the possibility of reversible assembly, plasmonic chirality in the visible or in the near-infrared region requires the use of host templates with nanometer-scale dimensions. Nanopores displayed by anodic aluminum oxide (AAO) represent an excellent candidate, allowing precise control over the diameter of parallel channels, down to tens of nanometers, which can be subsequently etched. The confinement of PS-capped gold NPs into 60 nm AAO pores led to the formation of helical assemblies with variable interparticle distances and configurations, depending on the PS molecular weight.[58] In a further size reduction, the assembly of 4 nm gold NPs functionalized with dodecanethiol,[59] in combination with a block copolymer (BCP), resulted in hybrid composites confined inside 35 nm AAO channels. A varied polymorphism was generated, ranging from separated spheres to cylinders or disks, as well as single- or double-helices (Fig. 1A). Each type of product arises as the direct consequence of a specific NP loading. Remarkably, dark field single-particle CD spectroscopy performed upon releasing the obtained helical nanostructures from the AAO templates revealed optical activity in the near-infrared (NIR) region. This system presents however the fundamental drawback of lacking control over the handedness of NP-BCP chiral assemblies, thus randomly producing one or the other enantiomer in each cavity, with a similar overall content for both of them. Block copolymers are indeed another class of materials that can be used to create nanostructures reaching sub-100 nm resolution. Both interfacial interactions and the volume fraction of the constituents determine the obtained morphologies, which include lamellae, 1D arrays, or hexagonally packed cylindrical micelles, to name a few.[60] An important advantage of BCPs is related to avoiding the need for removing the template, since they could as well remain integrated as a part of the final substrate. Additionally, their polymeric nature gains leverage toward post-synthesis transformations like pattern stretching and shrinkage,[61] which can help introduce corrugation in the *z*-axis. These concepts highlight the potential of BCPs and similar materials as alternative templates for the self-assembly of colloidal NPs into meta-surfaces with (plasmonic) optical activity.

Asymmetry through deformation

Poly(dimethylsiloxane) (PDMS) films have been employed[62] as mechanically deformable substrates for inducing chiroptical activity on thin films of 13 nm achiral gold NPs, deposited by layer-by-layer (LBL) self-assembly. Compared to the direct orientation of the plasmonic elements such as silver nanowires onto substrates using spray-assisted alignment,[63] the chiral configuration can also be obtained as a final morphology that results from an initial macroscopic asymmetric strain. This strain is applied prior to the deposition of NPs under a deformed state by twisting and clamping a few centimeters long rectangular PDMS substrate (Fig. 1B). This way, an asymmetric helical deformation is created. Thereafter, gold NPs and poly(urethane) were alternatively adsorbed onto the PDMS substrate to form uniform layers that, upon PDMS relaxation and recovery of the planar state, underwent buckling and deformation into chiral structures. Apparent CD could be measured according to the handedness imposed by the

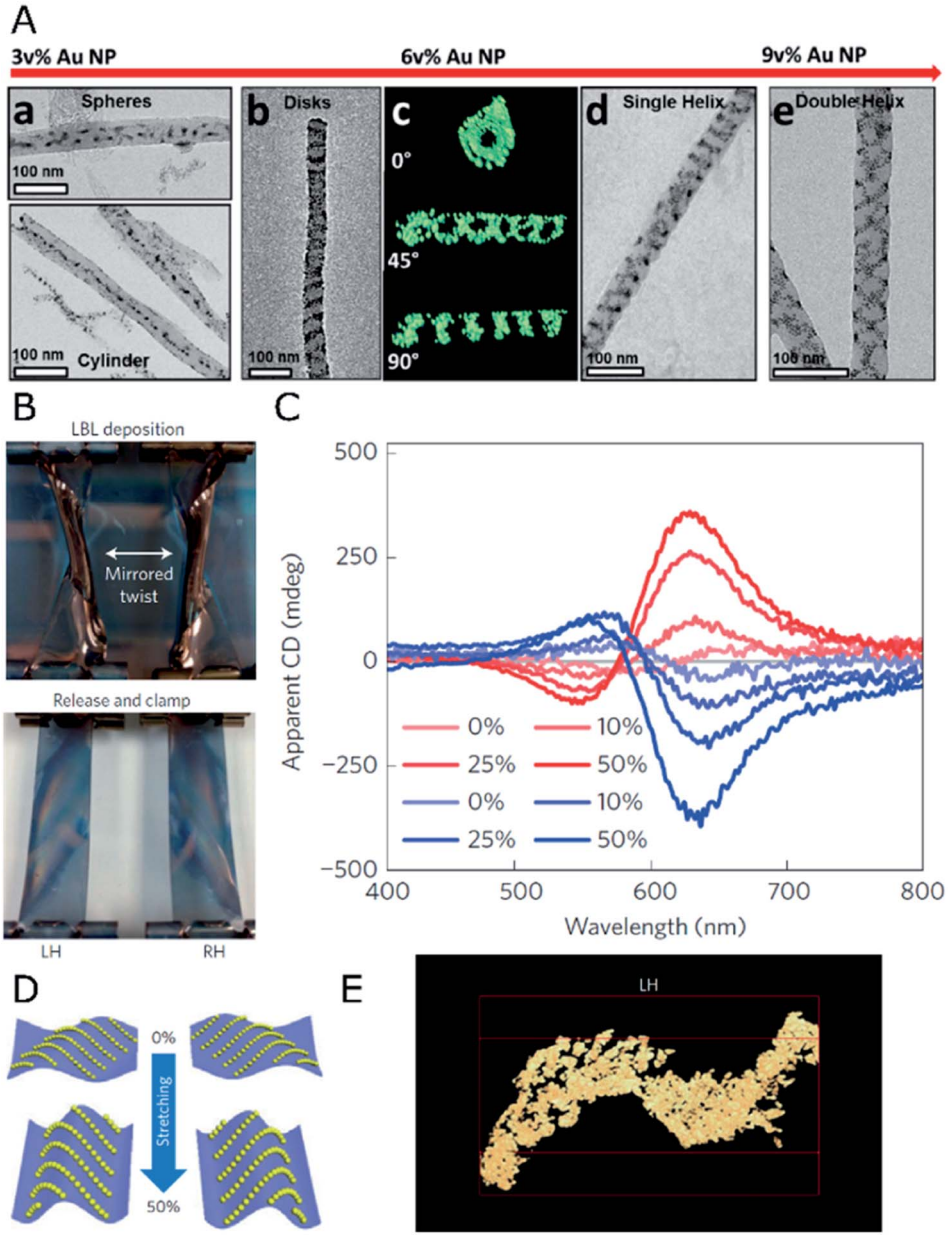

Fig. 1 (A) TEM and electron tomography of BCP-Au NP structures obtained for different NP loadings through co-assembly under confinement in AAO nanopores, displaying spherical and 1D arrays at 3 vol%, disks and single- or double-helices at 6 and 9 vol%, as labeled. Reproduced from ref. 59 with permission from American Chemical Society, copyright 2017. (B) Photographs of twisted, clamped PDMS substrates with opposite handedness after poly(urethane) and Au NP layer-by-layer deposition, and subsequent relaxation back into the planar state. (C) Apparent CD spectra for both (L- and R-, red and blue curves respectively) samples under different stretching percentages. (D) Scheme of NP arrangement in both samples under 0% and 50% stretching. (E) TEM tomograph showing the S-like surface topography of the cross-sectioned left-handed sample. (B–E) Reproduced from ref. 62 with permission from Nature Publishing Group, copyright 2016.

macroscopic twist (Fig. 1C). The key factor for this unconventional approach was a gradient in stress distribution along the bent surface, so that opposite compressive or tensile stresses acting on NPs located either on convex or concave areas were responsible for chirality transduction from the macro- to the nano-scale. Owing to the complex light–matter interactions taking place in strained and multicomponent aligned materials, contributions from linear effects (*e.g.*, linear dichroism (LD) and linear birefringence (LB)) characteristic of stretched solid-state films were considered. Besides initial bending as the source of an asymmetric arrangement of the NPs, the elastomeric properties of PDMS have been exploited to further modulate chiroptical activity through uniaxial stretching. Although interparticle distances (13 nm) were not affected by stretching, the optical activity in the system turned out to be enhanced by increasing the degree of strain (Fig. 1C). The reason behind this effect was an increased asymmetry of NP chains in the *z* axis, as a result of stretching and subsequent

compression along the *y* and *x* directions, respectively (Fig. 1D). The origin of chirality resided in the 3D S-like shape of Au NP chains under deformation (Fig. 1E). Thus, optical activity modulation by elastic deformations could be implemented in a reversible manner, establishing a clear precedent for the design of patterned systems with chiral and collective plasmonic effects.

Periodic templates

During the past decade, nanostructured PDMS has been used as a template of choice for the self-assembly and deposition of NPs under the action of capillary forces in receding menisci during solvent evaporation, thus allowing a precise and scalable deposition of NPs within various arrangements, ranging from single-particle architectures[64] to the construction of supercrystals.[65] Assembled NPs become regularly distributed over large areas, into one- or two-dimensional periodic arrays,[66,67] thereby generating hierarchical systems. Local close-packing allows the investigation of near-field plasmonic coupling,[68] while far-field effects may arise from the periodic distribution of NP clusters.[69] It should be mentioned that such periodic arrays can show system chirality as an extrinsic property for tilted light incidence.[70] This type of optical activity is a consequence of symmetry reduction for a specific pattern orientation. Notwithstanding, if plasmonic particles with intrinsic chirality can be used as the repeating units, lattice resonances could be obtained that are chiral in nature.[71] In this regard, template-assisted self-assembly may well represent a suitable strategy to construct meta-surfaces based on chiral repeating morphologies – which has been to date restricted to top-down lithographic approaches or multistep protocols – using achiral colloidal units. Similarly, the self-assembly of chiral NPs into periodical structures with long-range registry could benefit far-field optical phenomena and related applications.[34]

The surface nanostructuring of PDMS is typically carried out by soft lithography methods[72] such as replica molding of premade features, by drop casting and curing of PDMS. Alternatively, regular patterns can be created by the oxidation of previously stretched PDMS surfaces, by means of plasma treatment and subsequent relaxation. In such a process, the loss of elastomeric behavior for the vitrified upper surface layer translates into a sinusoidal corrugation of the material.[73] The dimensions and period of the formed wrinkles depend on the mechanical properties of the polymer, as well as on experimental conditions including plasma power, exposure time, and percentage of strain. Both strategies, wrinkle formation and replication of premade features, offer great versatility for template engineering and hint toward an effective modulation of the optical properties. Few examples in the literature give room to speculation about valid routes to achieve PDMS wrinkles with chiral morphologies. For instance, the modification of the fabrication methods resulted in zigzag patterns[74,75] and hierarchical wrinkled structures,[76,77] which could potentially facilitate asymmetry in three dimensions. In this respect, Hwang *et al.* reported the formation of chiral wrinkles by a sequence of stretching-oxidation steps along two different axes.[78] However, such chiral structures are not appropriate as templates for plasmonic chirality in the visible-NIR range since their dimensions fall on the microscale. Considering that the mechanical properties of PDMS nanostructures may impose a limitation on the formation of stable patterns below 100 nm, further miniaturization of chiral wrinkles would lead to a gradual increase in both relevance and complexity. However, a good number of advantages and precedents encourage further development of similar templated self-assembly strategies.

An elegant solution to the generation of chirality in self-assembled systems using PDMS as the template has been recently formulated by Fery and coworkers.[79] The design comprises a controllable and reversible chiral system based on 1D arrays of capillary-assisted self-assembled gold NPs on PDMS. Rather than relying on asymmetry from twisted morphologies or zigzag patterns, the authors stacked two layers of regular NP chains at oblique stacking angles (Fig. 2A). The superposed structures formed a chiral arrangement inducing optical activity of tunable magnitude and handedness, which was affected by the relative orientation of the layers (Fig. 2B). Two key factors lie behind an outstanding plasmonic chirality, with dissymmetry factors as high as 0.72. On one hand, the close-packing (~2 nm interparticle distances) of 77 nm gold NPs is enabled by the bottom-up technique of capillary-assisted self-assembly. On the other hand, stacking two elastomeric substrates together gave rise to reduced inter-layer distances of around 5 nm. Electromagnetic fields concentrate in the inter-layer space, making it possible to detect the presence of analytes (bovine serum albumin in this particular case) through a shift in the chiral resonances with state-of-the-art sensitivity (Fig. 2C). As an additional CD modulation possibility, the cross-stacked layers could be compressed, so that the stress induced by such a mechanical action on the elastomeric system translated into a deformation that effectively reduced longitudinal plasmon coupling along the chains. Consequently, the wavelength of those CD bands of longitudinal nature underwent a blue-shift and a loss of intensity (Fig. 2D).

Nanohelices and nanofibers as chiral templates

Symmetry breaking events have been reported for many different materials showing the ability to form nanoscaled helicoids, though obviously not all of them have been implemented for the assembly of plasmonic NPs. Among the most representative examples we can find hydrogel supramolecular systems, not only formed from chiral building blocks but also from achiral constituents, which have been used as templates to obtain Au nanowires,[80] or for the *in situ* growth of Au NPs by photoreduction.[81] Similar materials have been used to induce circularly polarized luminescence emission.[82] Tri- and di-block copolymers can also potentially form helical nanostructures and have thus been used as scaffolds, for instance templating the reduction of Pt with catalytic activity[83] or the assembly of achiral molecules into helical arrangements that gain optical activity.[84] Although the latter case involves thermal annealing

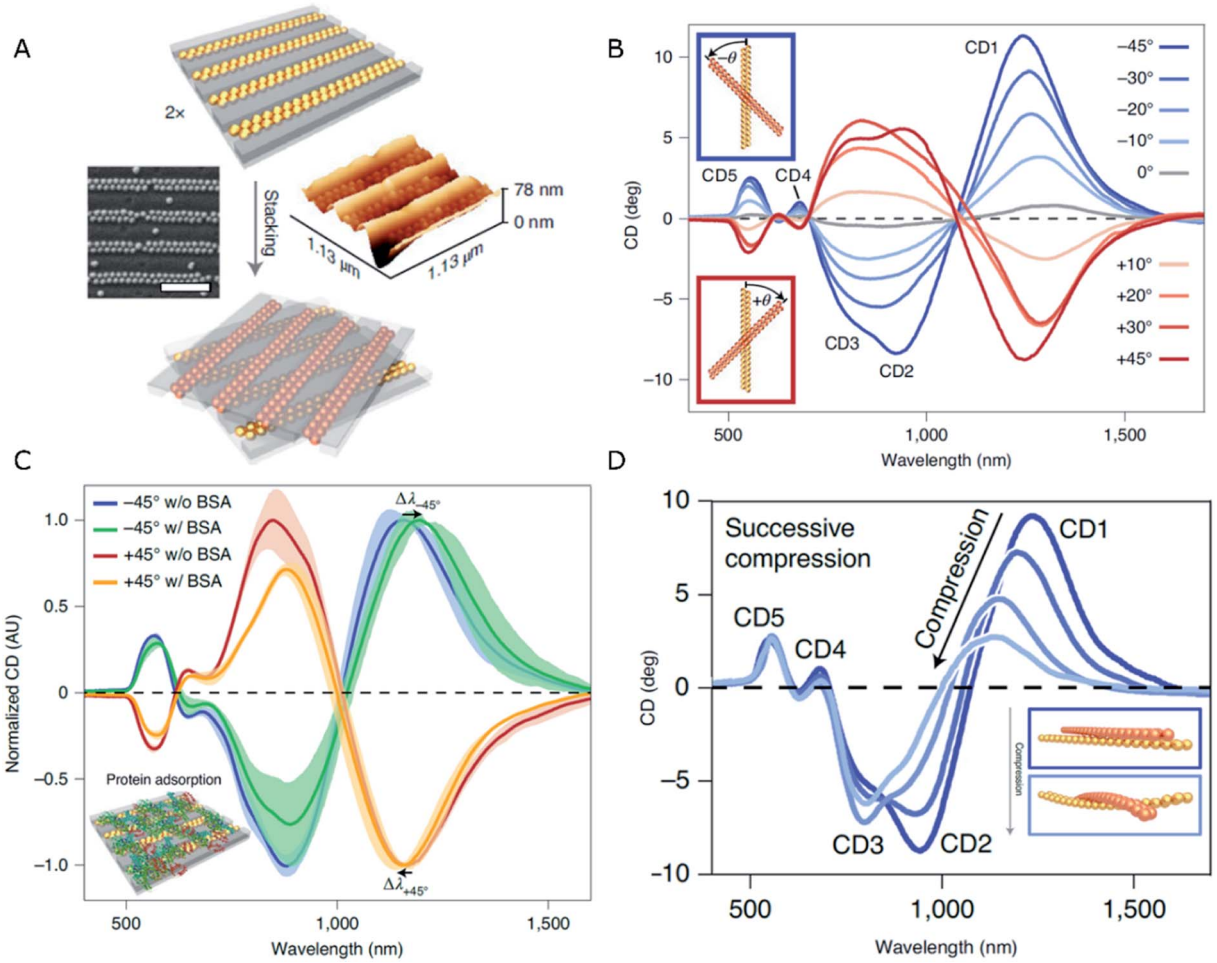

Fig. 2 (A) Schematics of the stacking method, and SEM and AFM characterization of dimer chains formed from Au NPs assembled on 1D patterned templates (scale bar is 500 nm). (B–D) CD spectra obtained for different stacking angles (B), in the presence of BSA (C), and upon compression applied normal to the stacking plane (D). Adapted from ref. 79 with permission from Nature Publishing Group, copyright 2021.

steps that might potentially result in the reshaping of anisotropic plasmonic NPs, it holds significant interest toward inducing chirality using chiral molecules as dopants. As an example, tartaric acid has been used to impose a specific handedness and tune the dimensions of BCP double helices.[84]

Liquid crystals

The integration of metal NPs into liquid crystal (LC) hybrid systems offers the opportunity to implement the characteristic responsiveness to external stimuli and the structural diversity of certain liquid crystal phases. For instance, a large family of cholesteric-based materials have been developed, including photo-responsive systems with tunable permittivity.[85] Chiral systems are not an exception and multiple examples of thermotropic and lyotropic liquid crystals have been reported to display chiral mesophases.[86–88] For instance, intrinsically chiral nanoscale cellulose rods and fibrils can self-assemble into stacked layers adopting chiral nematic organizations and show promising capacity as hosts for Au NPs.[89] However, in order to effectively "feel" the asymmetric distribution along the periodic twists of the cholesteric films and to maximize the collective coupling and chiroptical performance, plasmonic NPs should be localized in close proximity to each other.[90] Besides self-assembly, *in situ* reduction of gold ions would constitute another interesting route toward plasmonic-liquid crystal hybrid systems.[91]

A so-called helical nanofilament (HNF) phase,[92] or B4 phase, formed from bent-core mesogens, has been recently reported as a suitable chiral template. This phase owes its special interest to tunable and well-defined helical morphologies, together with a switching capacity upon temperature-driven structural changes. Although plasmonic optical activity is yet to be achieved for HNF systems, Lewandowski's group employed this chiral phase to template the self-assembly of gold nanospheres and nanorods (Fig. 3A–D).[93] In order to achieve sufficient affinity between the NPs and the LC molecules, while maintaining solubility in the isotropic phase, they were functionalized with chemically compatible organic ligands, which partially shared the bent-core molecular structure. The corresponding nucleation and growth processes of HNFs were not compromised by the presence of NPs, which ended up localized at the sides of the structure, stabilizing the air–HNF

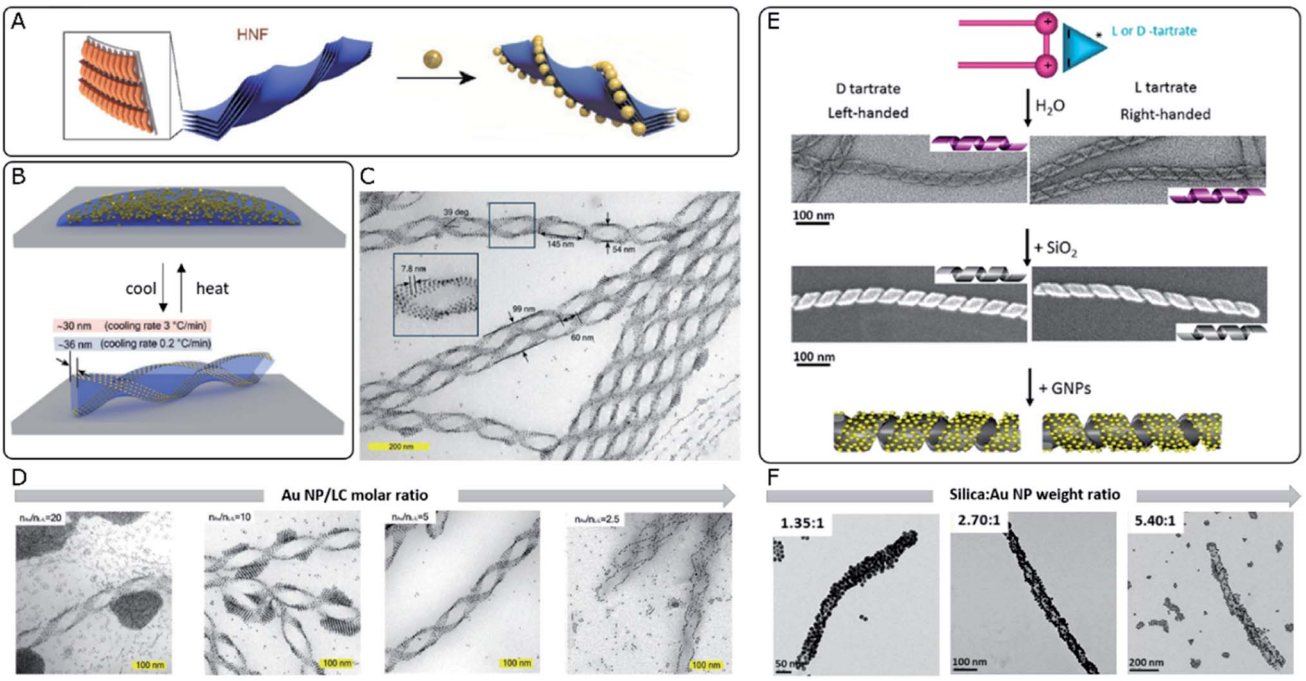

Fig. 3 (A) Schematic 3D model of stacked molecular layers of bent-core mesogens forming HNFs. Adapted from ref. 92 with permission from John Wiley and Sons, copyright 2020. (B) Schematic 3D illustration of the reversible formation of HNFs and simultaneous self-assembly of Au NPs upon cooling from the isotropic phase. (C and D) TEM characterization of LC–Au NP assemblies indicating their structural parameters (C) and the effect of decreasing the NP–LC molar ratio (D). (B–D) Reproduced from ref. 93 with permission from John Wiley and Sons, copyright 2019. (E) Schematic representation and TEM images of organic nanohelices formed from assembled surfactants, subsequent silica condensation and templated Au NP assembly. (F) TEM characterization showing the effect of increasing the silica–Au NP ratio (F). (E and F) Reproduced from ref. 40 with permission from American Chemical Society, copyright 2017.

boundaries. The result of the assembly was strongly dependent on the cooling rate from the isotropic phase (Fig. 3B), while the degree of coverage of the helices was tuned by adjusting the molar ratio between the organic matrix and the NPs (Fig. 3D). It should be taken into account that HNF phases undergo a spontaneous symmetry breaking process, where no preferential handedness is imposed at the nucleation stage from where the structures grow coherently into dendritic domains. Statistically, right- and left-handed HNFs are obtained with equal probability, giving rise to racemic samples. However, identification and mechanical removal of homochiral domains allow measuring plasmonic CD from micrometer-scale regions.[94] Interestingly, the introduction of an additive chiral dopant (sergeants and soldiers' effect) proved to be an effective chiral-selection strategy, acting at the nucleation stage and providing an enantiomeric excess of bent-core molecules forming HNFs.[95]

Silica nanohelices

Silica-based materials can support chirality-dependent interactions with enantiomeric molecules, which leads to chiral effects observed in either CD[96] or Raman spectroscopy.[97] Besides, their interest as unconventional templates for the self-assembly of achiral plasmonic NPs resides in the formation of chiral nematic structures[98] or silica nanohelices.[99] Oda's group has widely exploited the ability of amphiphilic molecules to self-assemble into twisted, helical, or tubular nanostructures in the presence of L- or D-tartrate counterions. Assembly takes place as a saddle-splay deformed superstructure, preserving the handedness imposed by the chiral molecule. Polymorphism may also occur, as a function of parameters like solvent choice, temperature, enantiomeric excess of tartrate ions, or aging time.[100] Interestingly, starting from such organic twisted ribbons as scaffolds, asymmetric silica structures can be obtained by sol–gel condensation of commonly used precursors like tetraethoxysilane (TEOS)[101] (Fig. 3E). These inorganic silica nanomaterials offer promising robustness and tunable surface functionality, to serve as templates for hybrid materials, as demonstrated through the self-assembly of polyoxomethalates,[102] Au NPs,[103] or the polymerization of fluorescent polymers.[104] Cheng *et al.*[40] reported the use of silica nanohelices as templates for the chiral self-assembly of Au NPs, bound through electrostatic interactions. In their system, Au NPs of sizes ranging between 4 and 10 nm were functionalized with either aminopropyltriethoxysilane (APTES) or carboxyl-terminated mercapto-oligo(ethylene glycol) ligands to acquire positive or negative surface charge, respectively. Bare silica helices could interact with APTES-functionalized NPs, whereas the functionalization of the template with NH_2 groups enabled the interaction with negatively charged NPs. The organization of the plasmonic units along the silica template was evidenced by TEM, as well as by a redshift of the plasmon resonance, thereby allowing the selection of optimal candidates. Besides

surface chemistry, assembly was shown to be affected by interparticle and particle–template interactions, which could be modulated by adjusting pH and the concentrations of each component. The extent to which the helical surface was covered by NPs could also be modified through the relative content (Fig. 3F). An optimal combination of the NP size, grafting density and interparticle distance gave rise to CD signals with an opposite Cotton effect around the plasmon resonance wavelength. The authors investigated the effect of those parameters on the resulting optical activity and compared the experimental observations with electromagnetic simulations.

On a subsequent development, a ten-fold increase in the *g*-factor was reported by using covalent instead of electrostatic interactions between Au NPs and the surface of silica nanohelices.[105] Based on the latest findings about the dependence of the *g*-factor on the long-range organization of plasmonic particles,[34] this effect could be related to improved organization when covalent bonds were used to template the superstructures. Thin films of the material could be deposited on glass slides coated with a polymeric adhesive layer, where the negatively charged helices were adsorbed through electrostatic attraction. Interestingly, grazing incidence spraying allowed control over the orientation of the helices, which opened the way to a comparison with drop-casted samples that showed no preferential orientation. The authors confirmed that the *g*-factor remained unaffected, regardless of the sample condition (suspension, non-oriented or oriented deposition). Notwithstanding, LB and LD effects arise for one-dimensionally oriented samples. These interactions are not present for non-oriented samples but become predominant in the aligned system, inducing linear polarization of unpolarized incident light. Interhelix plasmonic interactions were further evaluated for multilayer systems separated by a polyelectrolyte layer.[105] The thickness of the spacer film was fine-tuned by successive layer-by-layer polyelectrolyte depositions, permitting Gao *et al.* to observe a complete damping of plasmonic CD for ensembles with interlayer distances comparable to the interparticle spacing, which indicated unfavorable perturbation of the collective chiral resonance. In another interesting application, silica nanoribbons with pitch dimensions around 90 nm constitute an example of chiral material that interacts electrostatically with human islet amyloid polypeptide (hIAPP), accelerating the kinetics of the fibrillation process and inducing the formation of shorter fibrils with reduced toxicity. It was reported that right-handed silica ribbons performed better than their left-handed counterparts, which was reasoned in terms of available binding sites for fibrillation, together with a structural mismatch that would promote pre-formed fibrils to break into shorter aggregates.[106]

Amyloid nanofibers

Amyloid proteins undergo aggregation into helical nanofibers that can as well fulfill the requirements for a chiral template. The rich polymorphism and direct implication on degenerative disorders has increased the interest on their structure and motivated abundant research efforts devoted to the study – and suppression – of amyloid fibrillation. The acquisition of chiroptical activity by plasmonic NPs adopting the helical configuration of amyloid fibers would be in agreement with the above-mentioned theoretical principles and experimental demonstrations. What makes the case of amyloids more stimulating is the fact that CD signals arising from collective plasmonic interactions in the presence of protein aggregates could serve as a simple and highly sensitive method for diagnosis. Indeed, chiroptical activity from nanorod assemblies onto α-synuclein fibrils was demonstrated by Kumar *et al.*,[107] using Au nanorods that adsorbed onto the aggregated protein template. The nanorods were found to coat the fibrils (Fig. 4A), resembling a double-helical structure (Fig. 4B). The state of the nanorod-fibril system was reflected in the changes of the extinction and CD spectra over the incubation time: the longitudinal plasmon band red-shifted indicating preferential tip-to-tip alignment of neighboring nanorods, whereas a bisignate CD signal at the plasmonic wavelength arose gradually, indicating gradual assembly. Such changes in the optical properties of Au nanorods were not observed when α-synuclein monomers were mixed with Au NRs, instead of fibrillated samples. The CD-based detection method was also successfully applied to both prion fibrils and brain homogenate samples, establishing a clear difference between the signals obtained for healthy controls compared with Parkinson's disease-affected samples (Fig. 4C and D). Future work in this direction should address more specific interactions between plasmonic units and amyloid fibrils, so as to improve selectivity. In a more recent study, gold NPs were employed to label aggregates, allowing the cryo-TEM characterization of multiple types of amyloid fibrils.[108] Interestingly, the authors tested the affinity of different capping ligands toward the fibrils, thereby paving the way toward more efficient self-assembly.

Both a longer average number of plasmonic units assembled into helical arrays and an unprecedentedly high *g*-factor were achieved by the assembly of Au nanorods with hIAPP.[34] The initial system consisted of hIAPP monomers bound to CTAB-coated nanorods through Au–S bonds, with cysteine thiol groups. Rather than relying on mature hIAPP fibrils as the templates for the chiral assembly of gold nanorods – which was shown to yield discrete pairs of twisted nanorods with negligible CD – the authors studied the fibrillation of hIAPP in the presence of plasmonic NPs. As result, fibrillation was accelerated and long-range organization of nanorods along the fibrils, in an end-to-end configuration, was obtained (Fig. 4E–G). Molecular dynamics simulations helped unravel the origin of such favorable interactions between peptides and CTAB layers and, more importantly, a drug screening protocol was implemented for the evaluation of potential hIAPP fibrillation inhibitors. The method was based on the correlation between the intensity of transmitted polarized light with the assembly state of Au nanorods and, hence, the presence of amyloid fibers. Using a cross-polarization optical setup, only red light was transmitted after being rotated by NR-hIAPP assemblies (Fig. 4H and I). Therefore, the addition of drugs was detected by the loss of transmitted red light (Fig. 4J).

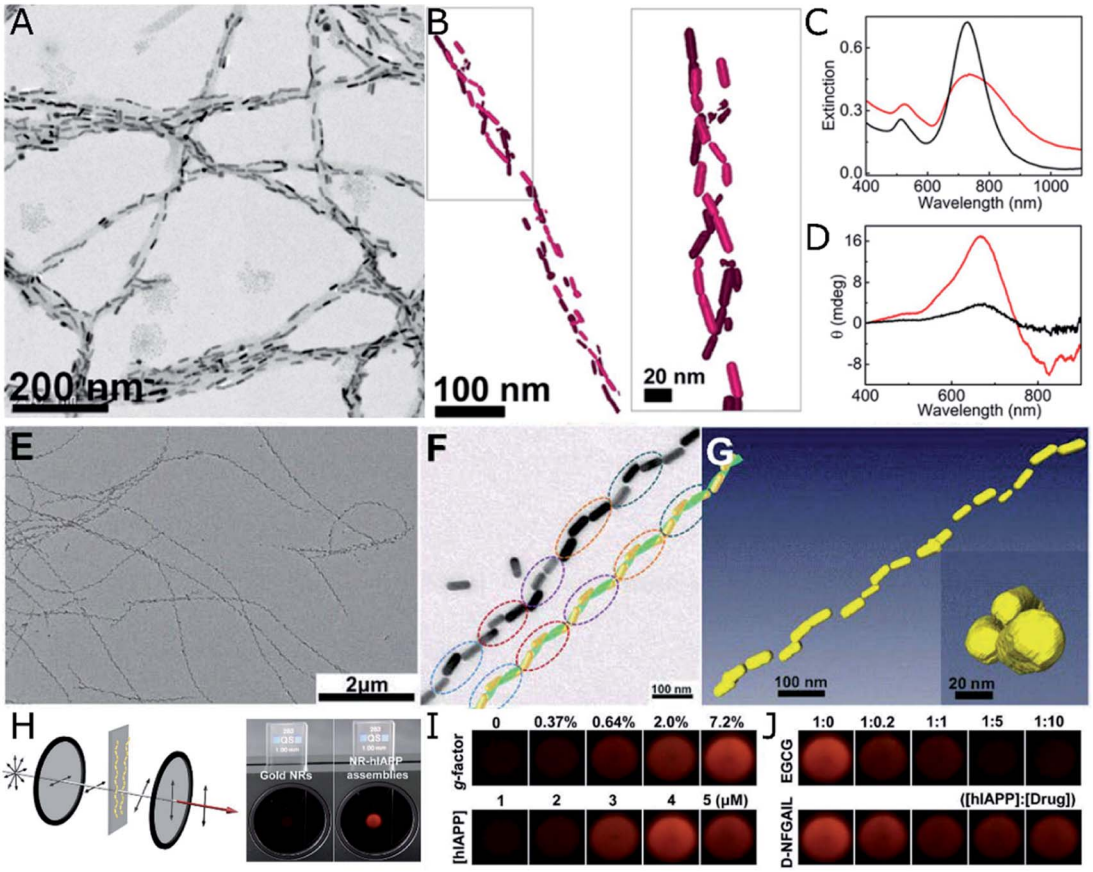

Fig. 4 (A–D) TEM (A) and cryo-TEM (B) characterization of Au nanorods assembled on α-synuclein fibrils. Extinction (C) and CD (D) spectra of Au nanorods after 30 min incubation with a control brain homogenate (black curves) and Parkinson's disease-affected brain (red curves). (A–D) Reproduced from ref. 107 with permission from National Academy of Sciences, copyright 2018. (E–J) TEM characterization of (E and F) Au nanorods assembled with hIAPP nanohelices. Reconstructed helical structures from TEM under various tilting angles (F) and from cryo-TEM tomography (G). Scheme of the cross-polarization optical setup and the differences in transmitted light between pure Au NPs (almost no transmission) and NR-hIAPP assemblies (intense red transmitted light) (H). Photographs of transmitted red light for AU-hIAPP assemblies with different *g*-factors and IAPP concentrations (I). Inhibition effect of increasing epigallocatechin gallate (EGCG) and D-NFGAIL peptide concentration translated into the loss of transmitted intensity (J). (E–J) Reproduced from ref. 34 with permission from The American Association for the Advancement of Science, copyright 2021.

Nanorods proved to be the morphology that better followed the helical trend of fibrillated hIAPP, resulting in *g*-factors that surpassed those achieved by the use of nanospheres or nanoarrows, by several orders of magnitude. The relationship between chiroptical activity and structural parameters was investigated experimentally and confirmed through finite-difference time-domain (FDTD) simulations. Nanorod dimensions of 50 nm in length and 19 nm in diameter were found to optimally match the helical structure of hIAPP fibrils. Larger particles could not be effectively incorporated along the helical features, leading to a decrease in the overall degree of order in the assembly. In contrast, chiral organization could still be observed for smaller nanorods, but with the *g*-factor decreasing upon reduction of the nanorod size.[34] The interparticle distance in Au nanorod-hIAPP helical assemblies was 5.8 ± 4.4 nm. Such a short spacing between adjacent plasmonic building blocks led to the strong coupling needed for collective chiral resonances to arise. The *g*-factor was additionally found to decrease when increasing the interparticle distance, in agreement with previous reports[40] and theoretical simulations.[109] This case study additionally allowed evaluating the dependence of optical activity on the number of helical turns, by repeatedly sonicating helical assemblies made of fibrils and rods. A drop in the *g*-factor was observed for broken fibrils made of less than four helical turns. The helical nanorods pitch is another important structural parameter, which in this case was of 160 nm, coinciding with that of hIAPP fibrils alone. Although it was not possible to modulate the pitch experimentally, the authors did simulate its effect on extinction and CD.

An even more versatile case study was presented by Rosi's group using peptide templates. Their approach, based on *in situ* nucleation and growth of NPs onto helical ribbon peptide structures, reached an important level of sophistication as a result of an important line of research.[39,43,110] Composed of a gold binding peptide and an aliphatic tail, the system is not directly connected to biosensing applications like the assembly with natural amyloid aggregates would be, but allows structural tuning of the resulting peptide template. The modification of

Table 1 Summarized information about the type, functionalization and interactions of Au NPs, template properties and optical activity for some of the most relevant self-assembly methods

Au nanoparticle (NP) size, shape	Surface ligand	Template	Interaction/ procedure	Tunability	Interparticle distance (nm)	Pitch (nm)	Width (nm)	Homochiral?	g-Factor	Ref.
4 nm spheres	Dodecanethiol (DDT)	35 nm AAO nanopores	Confinement	NP vol%	~4	20–50	30	No	—	59
16 nm spheres	Polystyrene (PS)	62 nm AAO nanopores	Confinement	PS mol weight	3.3–10.8	48 or 61	62	No	—	58
3.9 nm spheres	Liquid crystal (LC) ligand + DDT	LC	Helical nanofilament phase (HNF) transition	NP loading	7.8	145	54	No	—	93
23 nm quasi-spherical	LC ligand + DDT	LC	HNF transition	NP loading	2–3	300	44	No	—	94
4–10 nm spheres	PEG–tannic acid	Amine-grafted silica nanohelices	Electrostatic	NP size	2–3	~65	36	Yes	4.12×10^{-4}	40
10 nm spheres	Carboxylic acid	Amine-grafted silica nanohelices	Covalent	Film formation	14	108	20	Yes	4.4×10^{-3}	105
45 × 17 nm rods	Poly(vinyl-pyrrolidone)	Anthraquinone-based oxalamide fibers	Non-covalent	NP loading			$>10^2$	Yes	2.2×10^{-2}	45
50 × 19 nm rods	CTAB	hIAPP helical nanofibers	Au–S bond	NP size and loading	5.8	160	~40	Yes	0.12	34

the aliphatic tail length from 16 up to 22 CH_2 units was shown to affect both the helical pitch and the width of single helices, which inherently translated into different NP sizes since synthesis and assembly were interdependent processes. Higher g-factors were obtained for larger NPs – 13.4 nm and 15.9 nm – and smaller helical pitch lengths of 80 nm and 95 nm, respectively.[111]

Correlations between structure and optical activity

The wide variety of materials that can potentially serve as chiral templates unlocks access to multiple morphological and chemical possibilities. Representative information about the above-mentioned templates is collected in Table 1. The extensive research efforts in the field of chiral self-assembly allow us to establish various conceptual connections between the structure (Fig. 5A) and optical activity. Besides experimental evidence, different simulation strategies like the coupled dipole method,[40] discrete dipole approximation,[39,109] and electromagnetic calculations through the finite-element method or FDTD have been established to model plasmonic systems and evaluate their optical activity.[112] Altogether, some conclusions have been drawn for different template materials and will be summarized in this section.

Importantly, in chiroptical systems that owe optical activity to the self-assembly of plasmonic NPs, even non-bound building units that do not hinder CD would definitely reduce the overall g-factor of the system. Therefore, not only structural parameters must be optimized toward enhanced plasmonic coupling and more intense CD, but also an effective grafting of available NPs onto the templates is required. Optimized systems must minimize the number of unbound plasmonic units, while granting control over the degree of NP loading, which is an important parameter in self-assembly processes. Few-nanorod helical assemblies constructed with the help of DNA origami as the template showed stronger CD intensity for increasing average number of nanorods per ribbon,[112] as expected from theory.[27] Kotov and co-workers analyzed by FDTD simulations the impact of the number of nanorods on the absorbance and scattering contributions to the extinction of nanohelices under parallel or averaged orientations.[34] Several of the studies reviewed herein coincide in the observation of an optimal g-factor at a high template loading.[40,45] Naturally, NP dimensions and the interparticle distance within the assembled state are both related to NP loading. Extinction spectra indicate longitudinal coupling between assembled NPs through redshifts in the plasmon resonance wavelength. Such redshifts inform about the assembly taking place when both components are joined together,[40,107] and are sensitive to changes in the interparticle distance.[34,39] Strong dipole–dipole coupling between plasmonic NPs is required to obtain significant CD signals. Accordingly, an increased NP size and decreased interparticle distance would favor collective chiral plasmonic effects[40] arising in assembled systems (Fig. 5B and C), as long as the precise position of the units and overall asymmetric

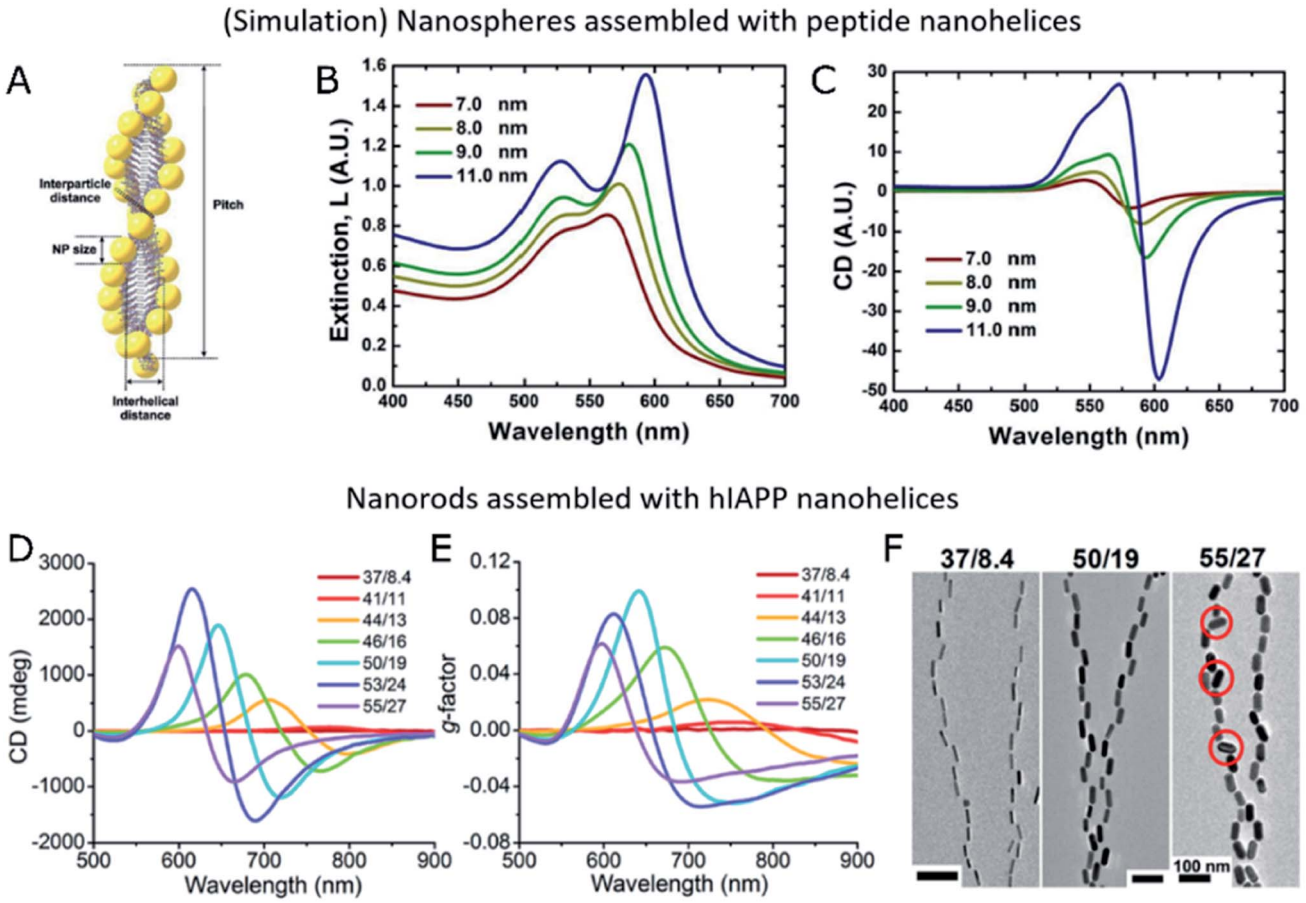

Fig. 5 (A–C) Schematic representation of Au NPs assembled into peptide nanohelices (A) and simulated extinction (B) and CD (C) for different NP diameters. (A–C) Reproduced from ref. 39 with permission from American Chemical Society, copyright 2013. (D–F) Experimental CD (D), *g*-factor (E) and TEM images (F) of Au nanorods of different sizes assembled with hIAPP nanofibers. (D–F) Reproduced from ref. 34 with permission from The American Association for the Advancement of Science, copyright 2021.

geometry of the system are not compromised[34] (Fig. 5D–F). Therefore, a rule of thumb for maximized *g*-factors would be increasing the size of NPs within the optimal range, to match the morphology of the template of choice. The same principle applies to the degree of loading of the template and, consequently, to the interparticle distance, which must preferably be as short as possible without reaching the contact between NPs. In the latter case, NPs could not be any longer considered as isolated dipoles and the system would be equivalent to a gold nanowire. It is also important to note that unbound NPs do not affect CD performance but inevitably diminish the *g*-factor of the samples.

More specific considerations can be made regarding the type of helical template. Two categories, namely single- and double-helices, are found among the multiple examples of helical templates. Transverse resonances between two intertwined helices can arise and increase in strength upon the reduction of the gap between both strands.[39] However, inter-helix interactions were calculated to be negligible elsewhere.[109] Another possibility for transverse resonances is the presence of more than one NP in width, as may occur for assemblies with liquid crystals[93] or helices formed under confinement inside AAO nanopores,[59] which could support interactions between parallel NP neighbors. Also, liquid crystal HNF phases have been shown to promote coherent alignment between neighboring helices (Fig. 3C), which could ideally enhance different collective plasmon coupling effects.

When considering the geometry of the template itself, the helical pitch is a relevant parameter that can strongly affect the asymmetry of the helices: long pitches translate into smooth twists resembling linear chains,[111] which implies a loss of asymmetry, while too short pitches can hinder effective helical alignment and, hence, proper plasmonic coupling. The NP size and the degree of packing onto the template are relevant toward evaluating the effect that the pitch length has on the relative positions and distances between plasmonic elements. In fact, the helical pitch may affect underloaded assemblies, since nonconsecutive NPs can be disposed into very different relative orientations, dictated by the separation and pitch length. That effect may even lead to parallel alignments (achiral plasmonic interaction) or an inversion of the CD sign,[34] thereby diminishing the overall optical asymmetry of the system. In sum, any template-NP combination can be optimized by improving the asymmetry of the template and its structural match with the

plasmonic building blocks, while an optimized assembly method must provide a precise control over NP loading.

Toward circularly polarized luminescence and plasmonic–excitonic systems

In analogy to the induction of chirality in plasmonic systems, CPL can arise from achiral emitters *via* different mechanisms, including chirality transfer from optically active molecules or asymmetric assemblies of achiral luminophores.[113] It should be noted, however, that circularly polarized light emission, often reported as CPL, may comprise circular polarization from both luminescence and scattering. The contribution from the latter is particularly strong in the case of noble metal plasmonic particles and optical media with chiral inhomogeneities, with dimensions comparable in size with the wavelength of the emitted light. While elaboration of the differences between these two processes is much needed, here we will primarily consider circularly polarized light emission as CPL, relegating the detailed discussion of a general case of differential optical activity of emitted photons to a later time.

Different approaches have demonstrated the transfer of chirality from host materials acting as templates to achiral luminescent guests. For instance, the confinement of 30 nm upconverting NPs inside chiral nanotubes resulted in a helical arrangement that conferred chirality to the upconverted emission.[114] Another example is the use of chiral silica grown onto complexes of polyethyleneimine–tartaric acid as a backbone, which allowed binding, complexation or *in situ* formation of different types of achiral emitters that became CD- and CPL-active.[115] Chirality transfer to achiral luminogens has been demonstrated by the use of a wide range of chiral templates, including gels made of supramolecular assemblies[116] and chiral smectic liquid crystal phases,[117] as well as metal–organic frameworks.[118] Once incorporated and organized within the chiral template, the achiral chromophores display CPL. A similar chirality transfer effect has been achieved with achiral semiconductor NPs. CPL induction has proven possible through co-assembly into supramolecular assemblies of chiral lipids[119] or chiral peptide dendron hydrogels.[120] The possibilities are not restricted to assembly, but also the templated synthesis of semiconductor NPs has been implemented using protein nanocages.[121]

A further increase in the size of the building units would make perovskite NPs relevant for this discussion. Perovskite NPs and related nanostructures have gained popularity as semiconductor emitters because of their outstanding photoluminescence properties combined with great synthesis versatility. In fact, *in situ* growth of perovskite NPs onto polymeric nanofibers acting as chiral templates[122] facilitates their assembly and acquisition of chiroptical properties. Assemblies of preformed perovskite NPs have also been reported employing amine-containing chiral lipids,[123] which form supramolecular lamellar structures. In this case, chirality is transferred from the template to the assembled emitters, with handedness being dictated and preserved by the gelation of the chiral lipid.

In summary, multiple materials can assume the role of chiral templates for CPL of either fluorescent molecules or different types of NPs. In order to consider the formation of hybrid materials composed of plasmonic and excitonic building units, the compatibility of assembly methods and the stability of each component are preliminary fabrication requisites. Potential advantages are provided by the typical size of quantum dots (a few nm) in comparison with typical plasmonic NPs (tens of nanometers), and examples of protocols for their co-assembly can already be found in the literature, regarding self-assembled CdTe NPs around Au nanorods.[49,124] Another key factor toward the design of synergistic composites and their optical properties would be the spectral overlap between plasmon modes and excitonic emission. Changes in the size of NPs due to quantum confinement or the modification of the halide composition of perovskite NPs allows tuning the emission wavelength along the visible range, making them advantageous candidates for plasmon–exciton coupling. The length of dielectric spacers (capping ligands or shell coatings) between chiral templates, or plasmonic NPs, and excitonic components is a crucial parameter to ensure efficient chirality transfer from the templates to the emitter guests and to avoid quenching of their photoluminescence, respectively. Template-assisted strategies for chiral self-assembly of plasmonic NPs are evaluated in this section as potential platforms for the fabrication of hybrid plasmonic–excitonic systems.

Large-scale patterned templates

We envision that assembled chiral morphologies may be obtained using patterned PDMS as a template by either (i) using chiral PDMS cavities or (ii) asymmetric pattern modification. The experimental realization of such a concept would provide access to the use of a wide variety of NPs of different sizes and shapes, as colloidal inks for evaporation-driven templated assembly, where surface chemistry plays a major role in affecting their stability and interactions. In fact, proper design of the different experimental conditions and surface functionalization should allow us to work simultaneously with two types of NPs and achieve a co-assembly. Considering that plasmonic NPs can be transferred into an organic phase, as well as the recent implementation of patterned PDMS to assemble $CsPbBr_3$ NPs dispersed in hexane,[125] the templated approach would be compatible with the use of organic solvents typically required to stabilize semiconductor emitters. Therefore, the use of patterned templates for the periodic arrangement of plasmon–exciton hybrid materials would benefit from the specific alignment of the individual constituents. Precedent work would be the 1D-assembly of CdSe–CdS core–shell nanorods showing anisotropic photoluminescence.[126]

Regarding large-scale templates, Kim *et al.* demonstrated the compatibility of their twisted PDMS strategy with different types of building blocks, including carbon nanotubes and polymer beads,[62] thus setting a promising starting point for hybrid materials including plasmonic–excitonic systems. The approach reported by Fery and co-workers[79] may also give room to the entrapment of emitters in the interlayer space accessing

superchiral hotspots. If necessary, dielectric spacers could be deposited through LBL assembly, to avoid quenching effects.

Helical templates

Stimuli responsiveness and tunable affinity toward different types of guest materials bring liquid crystal phases to the forefront of promising template candidates. Interestingly, HNF phases constructed from bent-core mesogens (host) have been proven to serve as templates for the chiral organization of achiral fluorescent molecules.[127] In order to be affected by the asymmetry of the template, fluorescent molecules should be part of a segregated nematic (N) domain formed from rod-like molecules (guest). This system had the appeal of being CPL-active only in the ⟨HNF/N⟩ phase, where HNFs act as the scaffold providing a chiral morphology, whereas the N domain can adapt to it. Thanks to the responsiveness of the N phase in the HNF network, CPL was obtained from aggregated fluorophores.[127] Although chiral properties were lost at room temperature upon N phase crystallization, this drawback could be overcome by using quantum dot building units with the ability (chemical compatibility) of directly interacting with HNFs, opening the way toward co-assemblies including Au NPs.

Proving the versatility of silica nanohelices as chiral templates, Oda's group went beyond Au NPs, demonstrating the covalent attachment of organic chromophores.[128] Optical activity in the UV region was induced as a result of the chiral organization of aggregated dyes, for which a high grafting density was crucial to ensure a close contact between emitters. Chiral self-assembly of $CsPbBr_3$ NPs on silica nanohelices was also achieved, using toluene as the solvent.[129] Interactions between perovskite NPs and the surface of the amine-functionalized silica template were not strong enough to guarantee a precise arrangement of the emitters in solution, whereas well-ordered chiral structures were found upon solvent drying. The latter case resulted in both CD and CPL activity. Making such a system compatible with the presence of helically arranged Au NPs would be a ground-breaking discovery. To date, the coupling of perovskite NPs with plasmonic NPs remains a challenge, with only a few reported studies that are limited to the decoration of perovskites with small (non-plasmonic) Au NPs. Simultaneous co-assembly may suffer from steric hindrance and incoherent chiral organization of each type of colloid. Therefore, a more appealing strategy would comprise an initial self-assembly of Au NPs into a gold helix[40] and then ensuring both the stability of the system in an organic solvent and Au-perovskite particle–particle interactions, through post-assembly functionalization of the exposed facets of the attached Au NPs. Alternative to multi-step assemblies, more straightforward approaches could be designed for the wide variety of herein reviewed templates, employing hybrid plasmonic–excitonic NPs.[130]

Conclusions

From the wide range of examples covered in this review, we can readily see that chiral assemblies of plasmonic NPs can be used as a convenient platform for biosensing of nanoscale biological structures including antibodies, viruses, exosomes, and other nanostructures. Long-range order has been demonstrated for the self-assembly of gold nanorods with amyloid fibers, showing great potential for drug discovery assays[34] and CD diagnosis of amyloid-related diseases.[107] Multiple routes have recently emerged toward achieving chiral assemblies of plasmonic nanoparticles by the use of both patterned and helical templates. On one hand, large-scale templated self-assembly of plasmonic NPs is a suitable strategy to design systems with mechano-tunable chiroptical activity,[62] which can be implemented as chiral sensing platforms.[79] As a stimulating next step, the versatility of such approaches could unlock compatibility with semiconductor counterparts, achieving their incorporation into chiral plasmonic–excitonic systems. On the other hand, helical phases displaying tailored geometrical features with potential to act as chiral templates can be obtained in confined BCP systems[59] or in certain LC phases[93,94] that undergo spontaneous symmetry breaking. Their implementation will depend on the effective manipulation of handedness, which is one of the current major challenges in the field. Silica nanohelices are well-stablished chiral templates,[40] which can additionally be chemically modified and transformed into thin films,[105] with high versatility for the combined self-assembly of Au NPs and perovskite NPs.[129] In summary, the state-of-the art knowledge on the collective chiroptical activity of colloidal plasmonic systems offers a large library of template materials, protocols, and theoretical background. Upcoming efforts rely on well-established structure–optical activity relationships, to maximize the chiroptical performance. Further studies on real-time tunable optical activity are expected to emerge in greater numbers during the next 10 years to satisfy the requirements for application of chiral photonic systems.

Author contributions

D. V.-L. wrote the first draft. All authors participated in the definition of the contents and in the revision and writing of the final manuscript.

Conflicts of interest

There are no conflicts to declare.

Acknowledgements

This work has been funded by the Spanish Ministerio de Ciencia e Innovación, through grant # PID2020-117779RB-I00 and the Maria de Maeztu Units of Excellence Program from the Spanish State Research Agency (Grant No. MDM-2017-0720). D. V.-L. acknowledges financial support from an FPI contract (PRE2018-084706) of the MICINN (Spain). N. A. K. expresses great thanks to the Vannevar Bush DoD Fellowship titled "Engineered Chiral Ceramics" ONR N000141812876.

References

1 A. Gogoi, S. Konwer and G.-Y. Zhuo, *Front. Chem.*, 2021, **8**, 611833.

2 M. Hentschel, M. Schäferling, X. Duan, H. Giessen and N. Liu, *Sci. Adv.*, 2017, **3**, e1602735.
3 J. Kumar, K. G. Thomas and L. M. Liz-Marzán, *Chem. Commun.*, 2016, **52**, 12555–12569.
4 M. Manoccio, M. Esposito, A. Passaseo, M. Cuscunà and V. Tasco, *Micromachines*, 2020, **12**, 6.
5 W. Chen, A. Bian, A. Agarwal, L. Liu, H. Shen, L. Wang, C. Xu and N. A. Kotov, *Nano Lett.*, 2009, **9**, 2153–2159.
6 W. Ma, L. Xu, A. F. de Moura, X. Wu, H. Kuang, C. Xu and N. A. Kotov, *Chem. Rev.*, 2017, **117**, 8041–8093.
7 X. Kong, L. V. Besteiro, Z. Wang and A. O. Govorov, *Adv. Mater.*, 2020, **32**, 1801790.
8 J. Kumar and L. M. Liz-Marzán, *Bull. Chem. Soc. Jpn.*, 2019, **92**, 30–37.
9 J. Guo, J.-Y. Kim, M. Zhang, H. Wang, A. Stein, C. B. Murray, N. A. Kotov and C. R. Kagan, *ACS Nano*, 2020, **14**, 1427–1435.
10 J. Yeom, U. S. Santos, M. Chekini, M. Cha, A. F. de Moura and N. A. Kotov, *Science*, 2018, **359**, 309–314.
11 Z. Cao, H. Gao, M. Qiu, W. Jin, S. Deng, K. Wong and D. Lei, *Adv. Mater.*, 2020, **32**, 1907151.
12 M. L. Solomon, A. A. E. Saleh, L. V. Poulikakos, J. M. Abendroth, L. F. Tadesse and J. A. Dionne, *Acc. Chem. Res.*, 2020, **53**, 588–598.
13 X. Wu, L. Xu, L. Liu, W. Ma, H. Yin, H. Kuang, L. Wang, C. Xu and N. A. Kotov, *J. Am. Chem. Soc.*, 2013, **135**, 18629–18636.
14 M. Grzelczak, L. M. Liz-Marzán and R. Klajn, *Chem. Soc. Rev.*, 2019, **48**, 1342–1361.
15 M. A. Boles, M. Engel and D. V. Talapin, *Chem. Rev.*, 2016, **116**, 11220–11289.
16 T. G. Schaaff and R. L. Whetten, *J. Phys. Chem. B*, 2000, **104**, 2630–2641.
17 Y. Zhou, M. Yang, K. Sun, Z. Tang and N. A. Kotov, *J. Am. Chem. Soc.*, 2010, **132**, 6006–6013.
18 G. Zheng, J. He, V. Kumar, S. Wang, I. Pastoriza-Santos, J. Pérez-Juste, L. M. Liz-Marzán and K.-Y. Wong, *Chem. Soc. Rev.*, 2021, **50**, 3738–3754.
19 H.-E. Lee, H.-Y. Ahn, J. Mun, Y. Y. Lee, M. Kim, N. H. Cho, K. Chang, W. S. Kim, J. Rho and K. T. Nam, *Nature*, 2018, **556**, 360–365.
20 G. González-Rubio, J. Mosquera, V. Kumar, A. Pedrazo-Tardajos, P. Llombart, D. M. Solís, I. Lobato, E. G. Noya, A. Guerrero-Martínez, J. M. Taboada, F. Obelleiro, L. G. MacDowell, S. Bals and L. M. Liz-Marzán, *Science*, 2020, **368**, 1472–1477.
21 J. Yeom, B. Yeom, H. Chan, K. W. Smith, S. Dominguez-Medina, J. H. Bahng, G. Zhao, W.-S. Chang, S.-J. Chang, A. Chuvilin, D. Melnikau, A. L. Rogach, P. Zhang, S. Link, P. Král and N. A. Kotov, *Nat. Mater.*, 2015, **14**, 66–72.
22 J.-Y. Kim, J. Yeom, G. Zhao, H. Calcaterra, J. Munn, P. Zhang and N. Kotov, *J. Am. Chem. Soc.*, 2019, **141**, 11739–11744.
23 Z. Hu, D. Meng, F. Lin, X. Zhu, Z. Fang and X. Wu, *Adv. Opt. Mater.*, 2019, **7**, 1801590.
24 A. O. Govorov, Z. Fan, P. Hernandez, J. M. Slocik and R. R. Naik, *Nano Lett.*, 2010, **10**, 1374–1382.
25 X. Mu, L. Hu, Y. Cheng, Y. Fang and M. Sun, *Nanoscale*, 2021, **13**, 581–601.
26 G. Shemer, O. Krichevski, G. Markovich, T. Molotsky, I. Lubitz and A. B. Kotlyar, *J. Am. Chem. Soc.*, 2006, **128**, 11006–11007.
27 Z. Fan and A. O. Govorov, *Nano Lett.*, 2010, **10**, 2580–2587.
28 W. Yan, L. Xu, C. Xu, W. Ma, H. Kuang, L. Wang and N. A. Kotov, *J. Am. Chem. Soc.*, 2012, **134**, 15114–15121.
29 W. Ma, H. Kuang, L. Wang, L. Xu, W.-S. Chang, H. Zhang, M. Sun, Y. Zhu, Y. Zhao, L. Liu, C. Xu, S. Link and N. A. Kotov, *Sci. Rep.*, 2013, **3**, 1934.
30 B. Auguié, J. L. Alonso-Gómez, A. Guerrero-Martínez and L. M. Liz-Marzán, *J. Phys. Chem. Lett.*, 2011, **2**, 846–851.
31 M. Song, L. Tong, S. Liu, Y. Zhang, J. Dong, Y. Ji, Y. Guo, X. Wu, X. Zhang and R.-Y. Wang, *ACS Nano*, 2021, **15**, 5715–5724.
32 Y. Nagaoka, R. Tan, R. Li, H. Zhu, D. Eggert, Y. A. Wu, Y. Liu, Z. Wang and O. Chen, *Nature*, 2018, **561**, 378–382.
33 Y. Zhou, R. L. Marson, G. van Anders, J. Zhu, G. Ma, P. Ercius, K. Sun, B. Yeom, S. C. Glotzer and N. A. Kotov, *ACS Nano*, 2016, **10**, 3248–3256.
34 J. Lu, Y. Xue, K. Bernardino, N.-N. Zhang, W. R. Gomes, N. S. Ramesar, S. Liu, Z. Hu, T. Sun, A. F. de Moura, N. A. Kotov and K. Liu, *Science*, 2021, **371**, 1368–1374.
35 Z. Ren and P.-X. Gao, *Nanoscale*, 2014, **6**, 9366.
36 X. Lan and Q. Wang, *Adv. Mater.*, 2016, **28**, 10499–10507.
37 J. Cheng, E. H. Hill, Y. Zheng, T. He and Y. Liu, *Mater. Chem. Front.*, 2018, **2**, 662–678.
38 X. Lu, W. Ye, W. You, H. Xie, Z. Hang, Y. Lai and W. Ni, *Phys. Rev. B*, 2020, **101**, 045431.
39 C. Song, M. G. Blaber, G. Zhao, P. Zhang, H. C. Fry, G. C. Schatz and N. L. Rosi, *Nano Lett.*, 2013, **13**, 3256–3261.
40 J. Cheng, G. Le Saux, J. Gao, T. Buffeteau, Y. Battie, P. Barois, V. Ponsinet, M.-H. Delville, O. Ersen, E. Pouget and R. Oda, *ACS Nano*, 2017, **11**, 3806–3818.
41 A. Kuzyk, R. Schreiber, Z. Fan, G. Pardatscher, E.-M. Roller, A. Högele, F. C. Simmel, A. O. Govorov and T. Liedl, *Nature*, 2012, **483**, 311–314.
42 X. Shen, C. Song, J. Wang, D. Shi, Z. Wang, N. Liu and B. Ding, *J. Am. Chem. Soc.*, 2012, **134**, 146–149.
43 S. Mokashi-Punekar, Y. Zhou, S. C. Brooks and N. L. Rosi, *Adv. Mater.*, 2020, **32**, 1905975.
44 C. Pigliacelli, R. Sánchez-Fernández, M. D. García, C. Peinador and E. Pazos, *Chem. Commun.*, 2020, **56**, 8000–8014.
45 A. Guerrero-Martínez, B. Auguié, J. L. Alonso-Gómez, Z. Džolić, S. Gómez-Graña, M. Žinić, M. M. Cid and L. M. Liz-Marzán, *Angew. Chem., Int. Ed.*, 2011, **50**, 5499–5503.
46 W. Feng, U. Kadiyala, J. Yan, Y. Wang, V. J. DiRita, J. S. VanEpps and N. A. Kotov, *Chirality*, 2020, **32**, 899–906.
47 J. Yan, W. Feng, J.-Y. Kim, J. Lu, P. Kumar, Z. Mu, X. Wu, X. Mao and N. A. Kotov, *Chem. Mater.*, 2020, **32**, 476–488.
48 N. Berova, L. D. Bari and G. Pescitelli, *Chem. Soc. Rev.*, 2007, **36**, 914.
49 T. Hu, B. P. Isaacoff, J. H. Bahng, C. Hao, Y. Zhou, J. Zhu, X. Li, Z. Wang, S. Liu, C. Xu, J. S. Biteen and N. A. Kotov, *Nano Lett.*, 2014, **14**, 6799–6810.

50 F. Wu, J. Guo, Y. Huang, K. Liang, L. Jin, J. Li, X. Deng, R. Jiao, Y. Liu, J. Zhang, W. Zhang and L. Yu, *ACS Nano*, 2021, **15**, 2292–2300.
51 J. Yuen-Zhou, S. K. Saikin, T. Zhu, M. C. Onbasli, C. A. Ross, V. Bulovic and M. A. Baldo, *Nat. Commun.*, 2016, **7**, 11783.
52 L.-Y. Wang, K. W. Smith, S. Dominguez-Medina, N. Moody, J. M. Olson, H. Zhang, W.-S. Chang, N. Kotov and S. Link, *ACS Photonics*, 2015, **2**, 1602–1610.
53 B. Yeom, H. Zhang, H. Zhang, J. I. Park, K. Kim, A. O. Govorov and N. A. Kotov, *Nano Lett.*, 2013, **13**, 5277–5283.
54 G. T. Pickett, M. Gross and H. Okuyama, *Phys. Rev. Lett.*, 2000, **85**, 3652–3655.
55 M. Tymczenko, L. F. Marsal, T. Trifonov, I. Rodriguez, F. Ramiro-Manzano, J. Pallares, A. Rodriguez, R. Alcubilla and F. Meseguer, *Adv. Mater.*, 2008, **20**, 2315–2318.
56 S. Ouhajji, B. G. P. van Ravensteijn, C. Fernández-Rico, K. S. Lacina, A. P. Philipse and A. V. Petukhov, *ACS Nano*, 2018, **12**, 12089–12095.
57 L. Jiang, J. W. J. de Folter, J. Huang, A. P. Philipse, W. K. Kegel and A. V. Petukhov, *Angew. Chem.*, 2013, **125**, 3448–3452.
58 S.-M. Jin, J. H. Hwang, K. Wang, J. Xu, I. Kim, J. Zhu and E. Lee, *Mater. Chem. Front.*, 2020, **4**, 3032–3039.
59 P. Bai, S. Yang, W. Bao, J. Kao, K. Thorkelsson, M. Salmeron, X. Zhang and T. Xu, *Nano Lett.*, 2017, **17**, 6847–6854.
60 C. Cummins, R. Lundy, J. J. Walsh, V. Ponsinet, G. Fleury and M. A. Morris, *Nano Today*, 2020, **35**, 100936.
61 J. Y. Kim, H. Kim, B. H. Kim, T. Chang, J. Lim, H. M. Jin, J. H. Mun, Y. J. Choi, K. Chung, J. Shin, S. Fan and S. O. Kim, *Nat. Commun.*, 2016, **7**, 12911.
62 Y. Kim, B. Yeom, O. Arteaga, S. Jo Yoo, S.-G. Lee, J.-G. Kim and N. A. Kotov, *Nat. Mater.*, 2016, **15**, 461–468.
63 H. Hu, M. Pauly, O. Felix and G. Decher, *Nanoscale*, 2017, **9**, 1307–1314.
64 H. Zhang, C. Kinnear and P. Mulvaney, *Adv. Mater.*, 2020, **32**, 1904551.
65 C. Hanske, G. González-Rubio, C. Hamon, P. Formentín, E. Modin, A. Chuvilin, A. Guerrero-Martínez, L. F. Marsal and L. M. Liz-Marzán, *J. Phys. Chem. C*, 2017, **121**, 10899–10906.
66 Y. Yu, C. Ng, T. A. F. König and A. Fery, *Langmuir*, 2019, **35**, 8629–8645.
67 C. Hanske, E. H. Hill, D. Vila-Liarte, G. González-Rubio, C. Matricardi, A. Mihi and L. M. Liz-Marzán, *ACS Appl. Mater. Interfaces*, 2019, **11**, 11763–11771.
68 C. Hanske, M. Tebbe, C. Kuttner, V. Bieber, V. V. Tsukruk, M. Chanana, T. A. F. König and A. Fery, *Nano Lett.*, 2014, **14**, 6863–6871.
69 C. Matricardi, C. Hanske, J. L. Garcia-Pomar, J. Langer, A. Mihi and L. M. Liz-Marzán, *ACS Nano*, 2018, **12**, 8531–8539.
70 E. S. A. Goerlitzer, A. S. Puri, J. J. Moses, L. V. Poulikakos and N. Vogel, *Adv. Opt. Mater.*, 2021, **9**, 2100378.
71 E. S. A. Goerlitzer, R. Mohammadi, S. Nechayev, K. Volk, M. Rey, P. Banzer, M. Karg and N. Vogel, *Adv. Mater.*, 2020, **32**, 2001330.
72 T. W. Odom, J. C. Love, D. B. Wolfe, K. E. Paul and G. M. Whitesides, *Langmuir*, 2002, **18**, 5314–5320.
73 A. Schweikart and A. Fery, *Microchim. Acta*, 2009, **165**, 249–263.
74 J. Yin, J. L. Yagüe, D. Eggenspieler, K. K. Gleason and M. C. Boyce, *Adv. Mater.*, 2012, **24**, 5441–5446.
75 P.-C. Lin and S. Yang, *Appl. Phys. Lett.*, 2007, **90**, 241903.
76 J.-H. Lee, H. W. Ro, R. Huang, P. Lemaillet, T. A. Germer, C. L. Soles and C. M. Stafford, *Nano Lett.*, 2012, **12**, 5995–5999.
77 Y. Li, S. Dai, J. John and K. R. Carter, *ACS Appl. Mater. Interfaces*, 2013, **5**, 11066–11073.
78 M. Hwang, C. Kim, J. Kim, J. G. Son and B. Yeom, *Adv. Funct. Mater.*, 2019, **29**, 1808979.
79 P. T. Probst, M. Mayer, V. Gupta, A. M. Steiner, Z. Zhou, G. K. Auernhammer, T. A. F. König and A. Fery, *Nat. Mater.*, 2021, **20**, 1024–1028.
80 M. Nakagawa and T. Kawai, *J. Am. Chem. Soc.*, 2018, **140**, 4991–4994.
81 S. H. Jung, J. Jeon, H. Kim, J. Jaworski and J. H. Jung, *J. Am. Chem. Soc.*, 2014, **136**, 6446–6452.
82 D. N. Nadimetla, M. Al Kobaisi, S. T. Bugde and S. V. Bhosale, *Chem. Rec.*, 2020, **20**, 793–819.
83 S. Tjaberings, M. Heidelmann, A. Tjaberings, A. Steinhaus, S. Franzka, B. Walkenfort and A. H. Gröschel, *ACS Appl. Mater. Interfaces*, 2020, **12**, 39586–39594.
84 X. Lu, J. Li, D. Zhu, M. Xu, W. Li and Q. Lu, *Angew. Chem., Int. Ed.*, 2018, **57**, 15148–15152.
85 A. Bhardwaj, V. Sridurai, S. A. Bhat, C. V. Yelamaggad and G. G. Nair, *Nanoscale Adv.*, 2021, **3**, 2508–2515.
86 J. Sato, K. Sugimura, Y. Teramoto and Y. Nishio, *Polymer*, 2019, **173**, 172–181.
87 L. Wang, A. M. Urbas and Q. Li, *Adv. Mater.*, 2020, **32**, 1801335.
88 C. Duan, Z. Cheng, B. Wang, J. Zeng, J. Xu, J. Li, W. Gao and K. Chen, *Small*, 2021, **17**, 2007306.
89 A. Querejeta-Fernández, G. Chauve, M. Methot, J. Bouchard and E. Kumacheva, *J. Am. Chem. Soc.*, 2014, **136**, 4788–4793.
90 A. Querejeta-Fernández, B. Kopera, K. S. Prado, A. Klinkova, M. Methot, G. Chauve, J. Bouchard, A. S. Helmy and E. Kumacheva, *ACS Nano*, 2015, **9**, 10377–10385.
91 S. A. Bhat, D. S. S. Rao, S. K. Prasad and C. V. Yelamaggad, *Nanoscale Adv.*, 2021, **3**, 2269–2279.
92 W. Lewandowski, N. Vaupotič, D. Pociecha, E. Górecka and L. M. Liz-Marzán, *Adv. Mater.*, 2020, **32**, 1905591.
93 M. Bagiński, M. Tupikowska, G. González-Rubio, M. Wójcik and W. Lewandowski, *Adv. Mater.*, 2020, **32**, 1904581.
94 P. Szustakiewicz, N. Kowalska, D. Grzelak, T. Narushima, M. Góra, M. Bagiński, D. Pociecha, H. Okamoto, L. M. Liz-Marzán and W. Lewandowski, *ACS Nano*, 2020, **14**, 12918–12928.
95 M. R. Tuchband, D. Chen, B. Horanyi, M. Shuai, Y. Shen, E. Korblova, D. M. Walba, N. Kapernaum,

F. Giesselmann, M. A. Glaser, J. E. Maclennan and N. A. Clark, *Liq. Cryst.*, 2016, **43**, 1083–1091.
96 Y. Huang, X. Vidal and A. E. Garcia-Bennett, *Angew. Chem.*, 2019, **131**, 10975–10978.
97 H. Kong, X. Sun, L. Yang, X. Liu, H. Yang and R.-H. Jin, *Anal. Chem.*, 2020, **92**, 14292–14296.
98 K. E. Shopsowitz, H. Qi, W. Y. Hamad and M. J. MacLachlan, *Nature*, 2010, **468**, 422–425.
99 H. Jin, Z. Liu, T. Ohsuna, O. Terasaki, Y. Inoue, K. Sakamoto, T. Nakanishi, K. Ariga and S. Che, *Adv. Mater.*, 2006, **18**, 593–596.
100 A. Brizard, C. Aimé, T. Labrot, I. Huc, D. Berthier, F. Artzner, B. Desbat and R. Oda, *J. Am. Chem. Soc.*, 2007, **129**, 3754–3762.
101 T. Delclos, C. Aimé, E. Pouget, A. Brizard, I. Huc, M.-H. Delville and R. Oda, *Nano Lett.*, 2008, **8**, 1929–1935.
102 M. Attoui, E. Pouget, R. Oda, D. Talaga, G. Le Bourdon, T. Buffeteau and S. Nlate, *Chem.–Eur. J.*, 2018, **24**, 11344–11353.
103 R. Tamoto, S. Lecomte, S. Si, S. Moldovan, O. Ersen, M.-H. Delville and R. Oda, *J. Phys. Chem. C*, 2012, **116**, 23143–23152.
104 S. Pathan, H. Noguchi, N. Yamada, Y. Kuwahara, M. Takafuji, R. Oda and H. Ihara, *Chem. Lett.*, 2019, **48**, 1088–1091.
105 J. Gao, W. Wu, V. Lemaire, A. Carvalho, S. Nlate, T. Buffeteau, R. Oda, Y. Battie, M. Pauly and E. Pouget, *ACS Nano*, 2020, **14**, 4111–4121.
106 A. Faridi, Y. Sun, Y. Okazaki, G. Peng, J. Gao, A. Kakinen, P. Faridi, M. Zhao, I. Javed, A. W. Purcell, T. P. Davis, S. Lin, R. Oda, F. Ding and P. C. Ke, *Small*, 2018, **14**, 1802825.
107 J. Kumar, H. Eraña, E. López-Martínez, N. Claes, V. F. Martín, D. M. Solís, S. Bals, A. L. Cortajarena, J. Castilla and L. M. Liz-Marzán, *Proc. Natl. Acad. Sci. U.S.A.*, 2018, **115**, 3225–3230.
108 U. Cendrowska, P. J. Silva, N. Ait-Bouziad, M. Müller, Z. P. Guven, S. Vieweg, A. Chiki, L. Radamaker, S. T. Kumar, M. Fändrich, F. Tavanti, M. C. Menziani, A. Alexander-Katz, F. Stellacci and H. A. Lashuel, *Proc. Natl. Acad. Sci. U.S.A.*, 2020, **117**, 6866–6874.
109 Q. Zhang, J. Gu, L. Zhang and J. Lin, *Nanoscale*, 2019, **11**, 474–484.
110 S. Mokashi-Punekar and N. L. Rosi, *Part. Part. Syst. Char.*, 2019, **36**, 1800504.
111 S. Mokashi-Punekar, A. D. Merg and N. L. Rosi, *J. Am. Chem. Soc.*, 2017, **139**, 15043–15048.
112 X. Lan, X. Lu, C. Shen, Y. Ke, W. Ni and Q. Wang, *J. Am. Chem. Soc.*, 2015, **137**, 457–462.
113 Y. Sang, J. Han, T. Zhao, P. Duan and M. Liu, *Adv. Mater.*, 2020, **32**, 1900110.
114 X. Jin, Y. Sang, Y. Shi, Y. Li, X. Zhu, P. Duan and M. Liu, *ACS Nano*, 2019, **13**, 2804–2811.
115 S. Tsunega, R. Jin, T. Nakashima and T. Kawai, *ChemPlusChem*, 2020, **85**, 619–626.
116 Y. Sang, D. Yang, Z. Shen, P. Duan and M. Liu, *J. Phys. Chem. C*, 2020, **124**, 17274–17281.
117 F. Song, Y. Cheng, Q. Liu, Z. Qiu, J. W. Y. Lam, L. Lin, F. Yang and B. Z. Tang, *Mater. Chem. Front.*, 2019, **3**, 1768–1778.
118 C. Zhang, Z. Yan, X. Dong, Z. Han, S. Li, T. Fu, Y. Zhu, Y. Zheng, Y. Niu and S. Zang, *Adv. Mater.*, 2020, **32**, 2002914.
119 S. Huo, P. Duan, T. Jiao, Q. Peng and M. Liu, *Angew. Chem., Int. Ed.*, 2017, **56**, 12174–12178.
120 C. Li, X. Jin, T. Zhao, J. Zhou and P. Duan, *Nanoscale Adv.*, 2019, **1**, 508–512.
121 M. Naito, K. Iwahori, A. Miura, M. Yamane and I. Yamashita, *Angew. Chem., Int. Ed.*, 2010, **49**, 7006–7009.
122 B. Zhao, X. Gao, K. Pan and J. Deng, *ACS Nano*, 2021, **15**, 7463–7471.
123 Y. Shi, P. Duan, S. Huo, Y. Li and M. Liu, *Adv. Mater.*, 2018, **30**, 1705011.
124 Z. Zhu, J. Guo, W. Liu, Z. Li, B. Han, W. Zhang and Z. Tang, *Angew. Chem.*, 2013, **125**, 13816–13820.
125 D. Vila-Liarte, M. W. Feil, A. Manzi, J. L. Garcia-Pomar, H. Huang, M. Dçblinger, L. M. Liz-Marzán, J. Feldmann, L. Polavarapu and A. Mihi, *Angew. Chem., Int. Ed.*, 2020, **59**, 17750–17756.
126 T. Wang, J. Zhuang, J. Lynch, O. Chen, Z. Wang, X. Wang, D. LaMontagne, H. Wu, Z. Wang and Y. C. Cao, *Science*, 2012, **338**, 358–363.
127 B. Kim, H. Choi, J. Lee, F. Araoka and S. Choi, *Adv. Funct. Mater.*, 2019, **29**, 1903246.
128 A. Scalabre, A. M. Gutiérrez-Vílchez, Á. Sastre-Santos, F. Fernández-Lázaro, D. M. Bassani and R. Oda, *J. Phys. Chem. C*, 2020, **124**, 23839–23843.
129 P. Liu, W. Chen, Y. Okazaki, Y. Battie, L. Brocard, M. Decossas, E. Pouget, P. Müller-Buschbaum, B. Kauffmann, S. Pathan, T. Sagawa and R. Oda, *Nano Lett.*, 2020, **20**, 8453–8460.
130 V. Kumar, N. Nisika and M. Kumar, *Adv. Opt. Mater.*, 2021, **9**, 2001150.